Collective response of an array of rotating particles to fluctuating confining forces

G. Schliecker,* Y. Khidas, M. Ammi, and J.-C. Messager
Groupe Matière Condensée et Matériaux, Bâtiment 11A, Campus de Beaulieu, Université de Rennes I, F-35042 Rennes, France
(Received 2 December 1999)

We study the influence of fluctuations of confining forces on the rotation patterns in a dense array of cylinders. Our theoretical studies are motivated by new results from detailed time-resolved experimental measurements. In order to calculate the system's evolution in time at each moment, a molecular-dynamics code adapted to the system is developed. The numerical procedure is tested by a comparison with rigorous predictions derived analytically. The chain's reaction on oscillating confining forces is analyzed numerically for different typical cases. Our theoretical results reproduce the striking features of the experimental data. A quantitative analysis of the experimental data is performed by a computation of their power spectrum and of spatial and temporal correlation functions. From our comparison of the theoretical and experimental results we conclude that the experimental rotation patterns result of random superpositions of different steady-state patterns (''collective random walk'').

PACS number(s): 45.70.−n, 62.20.−x, 81.05.Rm

I. INTRODUCTION

Force distributions and the resulting frictional properties of dense granular media are subjects of great interest [1,2]. When a dense packing of spherical particles is moved without deformation on a sliding plane, collective rotations are built up in order to reduce the frictional resistance: at a contact between two particles, no dissipation takes place, when they simply roll against each other. In most nonartificial dense packings, however, these rotations are frustrated due to geometrical constraints. In two-dimensional disk assemblies, whenever three rotating disks are in mutual contact, at least one of the three contacts has to slide. This frustration of rotations has an important influence on the organization of the particles' rotations.

The simplest system with completely frustrated rotations is a one-dimensional confined array of cylinders on a sliding plane, moved at constant acceleration in its main direction. Theoretically, for a perfect system, the organization of the cylinders' rotations in their steady state is well understood [3,4]. Less is known about the temporal evolution of the system. This did not seem to be important, since measurements of a first experimental realization of the system were found to be in convincing agreement with theoretical steady-state predictions [5].

We refined the experimental setup in Ref. [5]. Our experimental device now enables us to investigate the temporal evolution of the rotational motion of the cylinders in greater detail. It has turned out that temporal fluctuations of external control parameters due to imperfections of the experimental system have an interesting and non-negligible influence on the rotational patterns [6]. Due to these fluctuations, a simple comparison with the steady-state properties of the perfect theoretical system could not be performed. They instead require a theoretical discussion, taking into account the temporal fluctuations of the external control parameters.

In this paper, we will present a detailed study of the cylinders' rotations for fluctuating confining forces. In particular, a theoretical approach adapted to the experimental situation is developed.

The paper is organized as follows. In Sec. II, the experimental setup is shortly introduced. Typical features of the experimental system will be presented.

Theoretical calculations are presented in Sec. III. A theoretical description of the system begins with a representation of the equations of motion in Sec. III A. Rigorous results for the system's evolution at constant external control parameters are derived analytically in Sec. III B. In order to study the system's reaction on fluctuating compressions, in Sec. III C a simplified molecular-dynamics code is developed. The temporal evolution of the rotations is determined numerically for constant control parameters first. The numerical results are checked by a quantitative comparison with the rigorous analytical predictions derived. The typical transition time of the experimental system is estimated, and all steady-state rotation velocities of the cylinders of the array are determined. Then the system's reaction to fluctuations of the compression of the chain is determined for typical cases. The numerical results are compared with the experimental data.

In Sec. IV, the temporal fluctuations of the experimentally measured rotation angles are analyzed quantitatively by means of their power spectrum and temporal autocorrelation functions. The results are found to be best described by a stationary stochastic process for the random velocities (*random walk*). From this hypothesis, further information about the experimentally nonaccessible short-time behavior of the fluctuations is derived.

II. EXPERIMENTAL RESULTS I: SPATIAL CORRELATIONS

The system investigated here is shown schematically in Fig. 1: a close packed chain of L hard-core cylinders is based on a horizontal plane moving with a constant velocity v_p from left to right. The array, indexed with $i=1,\ldots,L$, from left to right, is confined by horizontal forces at both ends.

*Present address: MPI for the Physics of Complex Systems, Nöthnitzer Str. 38, 01187 Dresden, Germany.

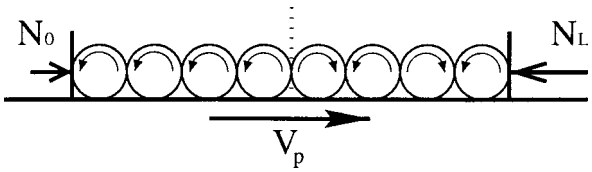

FIG. 1. The system considered here: a close-packed array of hard-core cylinders, confined by horizontal forces at the end of the chain, located on a horizontally moving plane.

Friction at the interparticle contacts and between the cylinders and the plane induces a complex behavior of the rotational motion of the particles.

Theoretically, at constant confining forces and shearing velocity, the system reaches a steady state with collective rotational modes after a transition time (cf. Fig. 1). The array of cylinders is subdivided into two spatial domains. In the first domain, on the left hand side, all the cylinders rotate in the same sense imposed by the motion of the plane. In this domain, the rotational velocities of neighboring cylinders are perfectly correlated. In the second domain, neighboring cylinders are counter-rotating, and their rotational velocities are perfectly anticorrelated [3].

For the investigation of the experimental system, the cylinders' rotation angles are obtained from marks on their fronts. We measure them automatically by a CCD camera connected to an image analysis with a time step δt. In order to gain detailed insight into the time evolution of the system, δt has been chosen as small as possible [6].

A polar representation of the measured angles in Fig. 2 gives an overview over the spatiotemporal behavior of the whole array: the radius and polar angle represent the time and rotation angle of each cylinder, respectively. The centers of the different circles represent the spatial positions of the cylinders. In Fig. 2, experimental results are represented for a total run of 6870 s with $\delta t = 9$ s. We have chosen a chain of ten Plexiglas cylinders with radii $R = 12.5$ mm and masses $m = 56.1$ g, rolling on a metallic plane with $v_p = 75$ μm/s. The chain has been confined by a cardboard block of 7.5 g on the left and a fixed wall on the right. Figure 2 shows that the left cylinders mainly follow the motion of the plane, whereas irregular fluctuations of the rotation angles can be observed on the right hand side. Due to these fluctuations, the relative tangential velocities at the contacts can hardly be estimated, neither from this representation nor from the total rotation angles as proposed in Ref. [5]. Furthermore, the time interval δt between the two measurements is restricted by the precision of the measured angles (about 1°). This prohibits a direct approach to instantaneous angular velocities. Nevertheless, as shown in Ref. [6], our detailed measurements allow us to deduce a counter-rotating behavior at the end of the chain, looking closer at the evolution of the rotation angles for neighboring cylinders.

FIG. 2. Polar representation of the temporal evolution of the rotation angles for the different cylinders. The cylinders' positions are represented as circles. The distance from a point of a curve to the center of its circle represents the time.

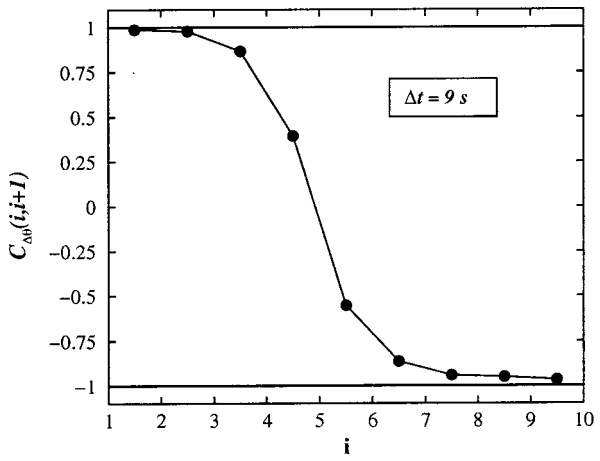

FIG. 3. Spatial correlations between the short-time rotation angles of neighboring cylinders.

An overview of the spatial correlations between rotations of different cylinders can be obtained from the cross-correlation function. This function constitutes a further tool for a characterization of a counter-rotating behavior. The cross correlation between the quantities f_i and f_j of two cylinders i and j is defined as

$$C_f(i,j) = \frac{\int dt\, f_i(t) f_j(t)}{\sqrt{\int dt\, f_i^2(t)}\sqrt{\int dt'\, f_j^2(t')}}, \qquad (1)$$

where the notation $\int dt \cdots := \int_0^T (dt/T) \ldots$, with the total integration time T, had been introduced. For $f_i(t) = \pm f_j(t)$, one obtains $C_f(i,j) = \pm 1$, reflecting strong (anti)correlations.

In order to estimate the correlations between the angular velocities of different cylinders, we have computed this function for the short-time rotation angles $f(t) = \Theta(t + \Delta t) - \Theta(t)$ of neighboring cylinders from the experimental data of Fig. 2. Theoretically, this spatial correlation function is discontinuous: it is equal to $+1$ in the first domain (cf. Fig. 1), with a jump to -1 in the counter-rotating domain. The experimental result for neighboring cylinders, $C_{\Delta\Theta}(i, i+1)$, is represented in Fig. 3. Whereas the strong correlations for $i \leqslant 3$ confirm our observations in Fig. 2, the strong anticorrelations at the right hand side quantify a nearly perfect counter-rotation. An intermediate behavior is given for $3 \leqslant i \leqslant 7$. This unexpected behavior and the continuous decrease at the right hand side will be analyzed here.

The experimentally observed strong (anti)correlations between the short-time rotation angles of neighboring cylinders for small (large) i are in good agreement with predictions from the steady-state analysis performed in Ref. [3]. However, neither the intermediate behavior in between nor the angular fluctuations at the end of the array can be obtained for constant horizontal compression, as supposed in Ref. [3]. Nevertheless, as shown in Ref. [6], these unexpected experimental features can be easily derived from the hypothesis of temporal superpositions of different steady-state patterns. In

Ref. [6], it was argued that these superpositions could be a consequence of fluctuations of the horizontal compression of the array due to imperfections in the cylindrical shape of the particles.

III. THEORY

In this section, we will present a quantitative theoretical investigation of the system under temporally fluctuating horizontal confining forces. To this end, the equations of motion for cylinders presented in Sec. III A will be integrated numerically. Such an analysis goes beyond the steady-state analysis for constant forces [3,4], since it requires a determination of the system's evolution in time at each moment. In Sec. III B, this evolution is studied first analytically for constant confining forces. The case of fluctuating confining forces will then be treated numerically in Sec. III C. To this end, the numerical simulations of the equations of motion will be performed with a simple molecular-dynamics code. The numerical code developed here is checked by a quantitative comparison of the simulation results with the analytical solutions from Sec. III B. Representative numerical results for oscillating horizontal compressions will be presented and discussed at the end of this section. They are compared with the experimental observations.

A. Equations of motion

We consider a dense horizontal packing of L parallel identical hard-core cylinders with radii R and masses m (see Fig. 1). The cylinders, based on a moving horizontal plane, are indexed from left to right with $i=1,\ldots,L$. The evolution of the cylinders' rotations is governed by the forces acting on the particles. The gravitational force of each cylinder is $\mathbf{G}=(0,-mg)$, where $g=9.81$ m/s is the gravitational acceleration. Further external forces are applied to the system vertically from the reaction of basal plane, and horizontally from the confining forces at both ends. The geometry of the close packing is not affected during the system's evolution. At the contacts, friction forces are mobilized when, due to the motion of the basal plane and/or the rotations of the cylinders, nonvanishing relative tangential velocities appear.

In order to simplify the formal representation in the following, the horizontal confining forces are considered to be exerted from particles with indices $i=0$ (left) and $i=L+1$ (right). The bottom will be represented as particle with index $i=L+2$. At interparticle and particle-plane contacts, we define the unit-distance normal vectors $\mathbf{n}_{ij}=-\mathbf{n}_{ji}$ and their corresponding tangent vectors $\mathbf{t}_{ij}=\mathbf{n}_{ij}\times(0,0,1)$, as represented in Fig. 4.

At the contact between two particles i and j, a normal force parallel to $\mathbf{n}_{ij}$, $\mathbf{N}_{ij}=N_{ij}\mathbf{n}_{ij}$, with $N_{ij}\geqslant 0$ appears. Our analysis will be restricted to cases where the geometry of the packing is not affected by the evolution of the system. Clearly, this condition allows one to consider only a restricted range of values for the external forces.

At interparticle contacts, tangential velocities of the cylinders' surfaces due to their rotational motion are denoted as $\mathbf{v}_i^t=v_i^t\mathbf{t}_{ij}$, $i=1,\ldots,L$. They are simply related to the angular velocities ω_i: $v_i^t=R\omega_i$. For the external contacts, we assume $v_0^t=v_{L+1}^t=0$ and $v_{L+2}^t=-v_p$, where v_p is the velocity of the moving plane.

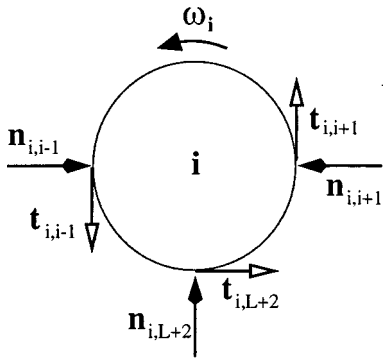

FIG. 4. Normal and tangential contact vectors of the ith cylinder.

Friction forces at the interparticle contacts play an essential role in the rotational motion of the cylinders. A nonvanishing relative tangential velocity $v_{ij}^r=v_i^t+v_j^t$ at a contact point $\langle i,j\rangle$ implies a friction force, which is (anti)parallel to the tangential vector at the contact: $\mathbf{T}_{ij}=T_{ij}\mathbf{t}_{ij}$. Following the friction law of Coulomb [7], the strength of this force is proportional to the normal force N_{ij}. As pointed out in Refs. [3,8], a closed contact $\langle ij\rangle$ remains sliding even at vanishing relative tangential velocity if $\dot{v}_{ij}^r\neq 0$. This leads to a generalized version of Coulomb's law for closed contacts in a dynamical system [8],

$$T_{ij}=-\mu_{ij}[\mathrm{sgn}(v_{ij}^r)+\delta_{v_{ij}^r,0}\ \mathrm{sgn}(\dot{v}_{ij}^r)]N_{ij}, \tag{2}$$

for $v_{ij}^r\neq 0$ or $\dot{v}_{ij}^r\neq 0$. Here we have introduced the signum function $\mathrm{sgn}(x):=|x|/x$ $(x\neq 0)$, $0(x=0)$. Whereas the first term in expression (2) represents Coulomb's friction law in its original version [7], the second term was suggested in Ref. [8]. The positive friction coefficients μ_{ij} are supposed to depend on the contacting materials, but not on the relative tangential velocities as, e.g., in Ref. [9]. They are μ between two cylinders, $\mu'':=\mu_{01}=\mu_{L,L+1}$ between the cylinders and the confining particles at the ends of the chain, and $\mu':=\mu_{i,L+2}$ between the cylinders and the plane. Expression (2) is valid only for sliding contacts, i.e., if the relative velocity or acceleration does not vanish. Otherwise, the contact becomes nonsliding, and the tangential contact force has to satisfy only the relation

$$|T_{ij}|\leqslant\mu_{ij}N_{ij}\quad\text{for}\quad v_{ij}^r=\dot{v}_{ij}^r=0. \tag{3}$$

We now turn to the *equations of motion*, governing the system's evolution in time. For each cylinder $i=1,\ldots,L$, we have two translational equations of motion and one rotational equation of motion for its translational velocity $\mathbf{v}_i$ and angular velocity ω_i. The equations of motion for the cylinders' translational velocities read

$$m\dot{\mathbf{v}}_i=\mathbf{G}+\sum_{j=0}^{L+2}\chi_{ij}(\mathbf{T}_{ij}+\mathbf{N}_{ij}),\quad i=1,\ldots,L. \tag{4}$$

Here we have introduced the characteristic function χ_{ij}: $\chi_{ij}=1$, if the particles i and j are in contact; otherwise $\chi_{ij}=0$. The condition of closed contacts requires that $\dot{\mathbf{v}}_i=\dot{\mathbf{v}}$

$=(\dot{v},0)$ for all cylinders. The rotational equations of motion do not explicitly depend on the normal contact forces:

$$(I/R)\dot{\omega}_i=\sum_{j=0}^{L+2}\chi_{ij}T_{ij},\quad i=1,\ldots L. \tag{5}$$

The moment of inertia I of a cylinder with homogeneous mass distribution is given by $I=mR^2/2$. Note that the cylinders considered in Eqs. (4) and (5) range from $i=1,\ldots,L$, whereas the summation over j also includes external particles, representing the confining walls and the bottom. Since we are concerned with cylinders of identical masses m, it is convenient to measure all forces in units of mg. Introducing the dimensionless forces $\mathbf{G}/(mg)=(0,-1)$, $\mathbf{T}_{ij}/(mg)$, and $\mathbf{N}_{ij}/(mg)$, Eqs. (4) and (5) read

$$\frac{d\mathbf{v}_i'}{dt'}=\frac{\mathbf{G}}{mg}+\sum_{j=0}^{L+2}\chi_{ij}\left(\frac{\mathbf{T}_{ij}}{mg}+\frac{\mathbf{N}_{ij}}{mg}\right),\quad i=1,\ldots,L \tag{6}$$

and

$$\frac{d\omega_i'}{dt'}=2\sum_{j=0}^{L+2}\chi_{ij}\frac{T_{ij}}{mg},\qquad i=1,\ldots,L, \tag{7}$$

with the dimensionless quantities $t':=tg/v_p$, $v_i':=v_i/v_p$, and $\omega_i':=\omega_i R/v_p$.

In this paper, we will focus on the experimental situation with $v_p=$const. and $dv_i'/dt'=0$. Thus the temporal evolution of the system is determined by the L values for the cylinders' angular accelerations $d\omega_i'/dt'$ only. They depend on the tangential contact forces [see expression (7)]. For a total number of N^{tot} contacts, there are $2N^{tot}$ values of the contact forces N_{ij} and T_{ij}. Consequently, the analysis of the system's evolution in time requires the determination of these $2N^{tot}+L$ quantities from the equations derived.

The equations of motion (4) and (5) or (6) and (7) form a set of $3L$ linear equations. They are integrated starting with an initial configuration of tangential velocities $\{v_i^t\}$. For all contacts with nonvanishing relative tangential velocities, the normal and tangential contact forces are uniquely related in expression (2). For each of the remaining contacts with vanishing relative tangential velocities, there are two possibilities: (a) For a *sliding* contact ($\dot{v}_{ij}^r\neq 0$), the contact forces are again related by expression (2). The sign of the relative angular acceleration $\dot{v}_{ij}^r$, input in expression (2) and resulting from expression (7), however, has to be determined self-consistently. (b) For each *nonsliding* contact, *inequality* (3) has to be satisfied. The condition $\dot{v}_{ij}^r=0$ yields a further equation, but with a maximum number of L linear independent equations. Thus, for fewer than L nonsliding contacts, N^{tot} independent equations can be obtained from expressions (2) and (3).

In the packing investigated here, the total number of contacts is given by $N^{tot}=2L+1$ (see Fig. 1). This yields a total number of $2N^{tot}+L=5L+2$ values of contact forces and angular accelerations. These quantities are governed by a maximum of $5L+1$ linear independent equations [(2), (3), (6), and (7)]. Thus only one free external parameter remains, e.g., the total horizontal compression of the chain. The maximum number of linear independent equations is obtained only when each cylinder has at least one sliding contact. Otherwise, we are left with the problem of an indetermination of contact forces, well known for higher-dimensional systems [1,10].

B. Analytical calculations for constant compression

In the following, the *temporal evolution* of the system at constant confining forces will be derived analytically. Our study will go beyond the analysis performed in Ref. [3], restricted to the steady-state properties for $\dot{v}=$const and $\dot{\omega}_i=$const. In the steady state, collective rotational modes along the chain are built up. For weak interparticle contact forces, an array with nonsliding cylinder-plane contacts is found (*phase I*), followed by an array of cylinders also rotating in the same sense, but with sliding contacts only (*phase II*). If the chain is long enough, at its end an array of cylinders operating in a counter-rotating mode (*phase III*) is built up. Here these studies will be extended analyzing the temporal evolution of the system to its steady state. We focus on the experimental situation where $\dot{v}_p, dv'/dt'=0$. In order to simplify the representation, the following notations are introduced: $N_i:=N_{i,i+1}/(mg)$, $T_i:=T_{i,i+1}/(mg)$, $R_i:=N_{i,L+2}/(mg)$, and $S_i:=T_{i,L+2}/(mg)$. In this notation, the equations of motion (6) and (7) reduce to

$$dv_i'/dt'=0=N_i-N_{i-1}-S_i, \tag{8}$$

$$R_i=1-T_i+T_{i-1} \tag{9}$$

$$(1/2)d\omega_i'/dt'=T_i+T_{i-1}+S_i,\quad i=1,\ldots,L. \tag{10}$$

Without loss of generality, we will assume from now on that all angular velocities are smaller than the velocity imposed by the plane, i.e., $\omega_i'\leqslant 1$. Thus from Coulomb's law [Eqs. (2) or (3)] and Eq. (9) we obtain the following relation for the cylinder-plane contact force S_i:

$$S_i\leqslant\mu'(1+T_{i-1}-T_i). \tag{11}$$

Equality holds for cylinders sliding on the plane, i.e., if $\omega_i'\neq 1$ or $d\omega_i'/dt'\neq 0$. Insertion of Eq. (10) into Eq. (11) yields the useful relation

$$(1/2)d\omega_i'/dt'\leqslant\mu'+(1-\mu')T_i+(1+\mu')T_{i-1}. \tag{12}$$

Possible solutions of the expressions (8)–(10) and (12) will now be discussed for two typical situations, where all contacts between neighboring cylinders are either sliding or nonsliding. In the steady state, phases I and II would correspond to sliding interparticle contacts, and phase III to nonsliding interparticle contacts.

1. Sliding interparticle contacts

We consider a cylinder i, and assume sliding contacts with its neighbors, i.e., $T_{i-1}=-\mu N_{i-1}$ and $T_i=-\mu N_i$. This enables us to calculate, from Eqs. (8) and (10), the following identity:

$$(\mu/2)d\omega_i'/dt'=(1+\mu)T_{i-1}-(1-\mu)T_i. \tag{13}$$

A combination of expressions (12) and (13) yields, after some elementary manipulations,

$$d\omega_i'/dt' \leqslant 4(T_{i-1}-T^*), \tag{14}$$

with

$$T^* := -\mu N^* := -\frac{\mu'}{2}\frac{(1-\mu)}{1-\mu\mu'}.$$

Equality is given if the cylinder slides on the plane, i.e., for $\omega_i'<1$. In this case, for a weak confining contact force $T_{i-1}>T^*$, a positive acceleration is obtained. The rotation velocity approaches the value $\omega_i'=1$, where the cylinder is rolling without friction on the plane. At this point, acceleration stops: the unique solution satisfying relation (14) is $d\omega_i'/dt'=0$. As can be easily checked, the assumption of a nonvanishing angular acceleration would always yield the opposite sign as solution. This shows clearly that phase II, requiring a steady-state solution with $d\omega_i'/dt'=\text{const}>0$ [3], has zero length in the case $\dot{v}=\dot{v}_p=0$.

As shown in Ref. [3], the possible steady-state solution ($\omega_i'=1, d\omega_i'/dt'=0$) can especially be achieved on the left hand side of the array, if the external confining force N_0 is weak enough. A closed array of particles in this steady state is built up, and thereby constitutes phase I. Since in this phase the interparticle contacts are sliding, all forces are uniquely determined. From Eq. (13) we obtain an exponential increase of the interparticle friction forces in phase I:

$$T_i=\left(\frac{1+\mu}{1-\mu}\right)^{i-1}T_1 \quad \text{with} \quad T_1=\frac{-\mu(1+\mu'')}{1-\mu}N_0.$$

For the first cylinder $i=L_1+1$ with contact force $T_{L_1}<T^*$, the steady-state solution no longer exists. Accordingly, the number of particles in the phase I, L_1, is given by

$$L_1 \leqslant 1-\frac{\ln(N_0/N^*)+\ln(1+\mu'')-\ln(1-\mu)}{\ln\{(1+\mu)/(1-\mu)\}}.$$

For $\mu=\mu''$, this expression agrees with the result for a nonaccelerated array in Ref. [3]. This result is exactly what one expects intuitively: for weak confining forces, the particle-plane contacts dominate, and the system reduces the loss of energy by friction at these contacts. For strong horizontal confining forces, however, the interparticle contacts dominate. Thus a counter-rotating behavior can be expected for this case.

2. Nonsliding interparticle contacts

We will now discuss possible solutions for a closed array of L_3 counter-rotating particles indexed with $i=i_0+1,\ldots,i_0+L_3$. As consequence of the perfect counter-rotations, the interparticle contacts are nonsliding ($v^r_{i,i+1}=\dot{v}^r_{i,i+1}=0$ for $i_0+1\leqslant i\leqslant L_3-1$). At the particle-plane contacts, friction is supposed to be mobilized. This enables us to determine all forces uniquely, especially since relations (11) and (12) hold with equality.

Although Coulomb's law does not hold in this case, a unique relation between the contact forces N_i and T_i can be derived. Inserting identity (11) into Eq. (8), after summation one obtains

$$N_i-N_{i_0}=\mu'(i-i_0)-\mu'(T_i-T_{i_0}) \tag{15}$$

for $i=i_0+1,\ldots,i_0+L_3$. At the left boundary of the counter-rotating array, we assume a sliding interparticle contact, $T_{i_0}=-\mu N_{i_0}$. The condition of a sliding contact at the right boundary, constituted by a cylinder or the confining wall, gives $T_{i_0+L_3}=\pm\mu_{L_3}N_{i_0+L_3}$. Here $\pm\mu_{L_3}$ is the shorthand notation of the product of the friction coefficient μ_{L_3} with the sign of the relative tangential velocity at the right end of the counter-rotating array. In fact, for a given value $\pm\mu_{L_3}$ *both* contact forces are fixed, as can be deduced from Eq. (15):

$$T_{i_0+L_3}=\pm\mu_{L_3}N_{i_0+L_3}=\frac{\pm\mu_{L_3}\{(1-\mu\mu')N_{i_0}+\mu'L_3\}}{1\pm\mu'\mu_{L_3}}.$$

The contacts forces T_{i_0} and $T_{i_0+L_3}$ (instead of μ_{L_3}) are considered here as the control parameters in the counter-rotating array.

The values T_i of the interparticle tangential contact forces can be evaluated explicitly from the nonsliding condition

$$d\omega'_{i_0+1+l}/dt'=(-1)^l d\omega'_{i_0+1}/dt' =: (-1)^l\dot{\omega},$$

valid for $l=0,\ldots,L_3-1$. For the counter-rotating array, identity (12) yields, after a few elementary manipulations,

$$T^{\oplus}_{i_0+l}=\frac{(-1)^l\dot{\omega}}{4\mu'}+(-\alpha)^l\left(T^{\oplus}_{i_0}-\frac{\dot{\omega}}{4\mu'}\right), \tag{16}$$

where $l=0,\ldots,L_3$. The notations $\alpha:=(1+\mu')/(1-\mu')$ and $T_i^{\oplus}:=T_i+\mu'/2$ have been introduced. So far, a similar result for the steady state of an accelerated array was derived in Ref. [3]. Without acceleration, however, more effort is needed to determine the steady-state velocities in phase III. In the following, we will show that in this case, a steady-state solution does not exist for sliding particle-plane contacts. Result (16) allows us to calculate the angular acceleration $\dot{\omega}$ from the control parameters T_{i_0} and $T_{i_0+L_3}$:

$$\frac{\dot{\omega}}{4\mu'}=\frac{(-1)^{L_3+1}T^{\oplus}_{i_0+L_3}+\alpha^{L_3}T^{\oplus}_{i_0}}{\alpha^{L_3}-1}. \tag{17}$$

It turns out that for given experimental parameters μ, μ', μ_{L_3}, and L_3, a vanishing angular acceleration is achieved only for one single value of T_{i_0}. Accordingly, a steady-state solution for the counter-rotating array with $\omega_i'<1$ exists only in singular cases.

Insertion of Eq. (17) in expression (16) yields the dependence of the internal tangential contact forces on the two external parameters:

$$T^{\oplus}_{i_0+l}=(-1)^l\{(1-p_l)T^{\oplus}_{i_0}+p_l(-1)^{L_3}T^{\oplus}_{i_0+L_3}\}, \tag{18}$$

where $l=0,\ldots,L_3$. The weights $p_l:=(\alpha^l-1)/(\alpha^{L_3}-1)$ increase monotonically from zero at $l=0$ to their maximum value of 1 at $l=L_3$. Accordingly, the quantities $(-1)^l T^{\oplus}_{i_0+l}$ vary monotonically from $T^{\oplus}_{i_0}$ to their value for $l=L_3$—with upper and lower bounds at the boundaries.

So far, the forces and accelerations have been determined analytically for the counter-rotating array. Results (17) and (18) enable us to check quantitatively the conditions under which this array can be built up, a point neglected in previous investigations [3].

The first restriction follows from the requirement, that the particles do not detach. Formally, this requires the positivity of the plane's reaction force: $R_i \geqslant 0$ in Eq. (9). In Ref. [3], the exponential increase of the $|T_{i_0+l}|$ in expression (16) gave rise to a restriction of the length L_3. Expression (18) shows instead that the lower and upper bounds of these forces are governed by μ' and the control parameters T_{i_0} and $T_{i_0+L_3}$. Thus, as long as $\mu', |T_{i_0}| \ll 1$, the positivity of R_i is guaranteed even for a long counter-rotating array, if $\mu' \mu_{L_3} L_3 \ll 1$. This relation is especially valid for *all* lengths L_3 if a frictionless wall is chosen $\mu_{L_3}=0$.

Finally, it remains to check the necessary condition $|T_i| \leqslant \mu N_i$ for nonsliding interparticle contacts. Making use of identity (15), this condition corresponds to upper and lower bounds for T_i,

$$T^{min}_{i_0+l} \leqslant T_{i_0+l} \leqslant T^{max}_{i_0+l}, \tag{19}$$

with $T^{min}_{i_0+l}:=T_{i_0}-l[\mu\mu'/(1-\mu\mu')]$ and $T^{max}_{i_0+l}:=-[(1-\mu\mu')/(1+\mu\mu')]T^{min}_{i_0+l}$. Clearly, a check of these conditions in expression (18) yields further restrictions on the friction forces T_{i_0} and $T_{i_0+L_3}$. Their formal derivation requires a separate investigation of various cases. Accordingly, its general representation here would be too involved. We have found that it is sufficient to restrict $T_{i_0+L_3}$ such that relation (19) holds for $l=L_3-1, L_3$. In particular, the latter case requires that $\mu_{L_3} \leqslant \mu$. For small values of l, only in a restricted range of values for T_{i_0} no contradictions of the nonsliding conditions appear. The most restrictive conditions are obtained for a long counter-rotating array, where $p_1 \approx 0$: $-T^{max}_{i_0+1} \leqslant T_{i_0}+\mu' \leqslant -T^{min}_{i_0+1}$. This yields, in particular, an estimate of the upper bound of T_{i_0}:

$$T_{i_0} \leqslant T^{**} = T^{*} + \frac{\mu(\mu')^2}{2(1-\mu\mu')}. \tag{20}$$

The bound T^{**} is slightly larger than T^{*} after expression (14). For small friction coefficients, both values become indistinguishable. Thus our intuitive expectation of a counter-rotating behavior at the right of the array building up phase I is confirmed.

To summarize, a counter-rotating array can be expected on the right-hand side of the chain, but with a nonvanishing angular acceleration [Eq. (17)] when the particle-plane friction is mobilized for all cylinders. Accordingly, particles with positive acceleration achieve an angular velocity $\omega'=1$. At this point, a steady-state solution with $\dot{\omega}=0$ no longer contradicts expression (17). Due to the additional nonsliding cylinder-plane contacts the forces are no longer uniquely determined in this counter-rotating steady state (*phase III*). We conclude that in phase III of a nonaccelerated array only two angular velocities exist: $\omega_i'=\pm 1$.

C. Numerical simulations

In the case of fluctuating confining forces, Eqs. (6) and (7) can no longer be treated analytically. However, their numerical integration is a complicated task when the relative tangential velocities vanish at several contacts. In this situation, all combinations of cases (a) and (b) discussed after Eqs. (6) and (7) have to be tested numerically. The fast converging *contact dynamics* algorithm was shown to be useful for the determination of the steady state of the system at constant nonvanishing acceleration $\dot{v} \neq 0$ [3]. In these numerical studies, a unique solution was always found. This observation has important consequences for the stability of nonsliding contacts. A nonsliding contact is stable if the solution $v^r_{ij}=\dot{v}^r_{ij}=0$ is approached from both sides: $v^r_{ij}=0^+ \Rightarrow \dot{v}^r_{ij}<0$ and $v^r_{ij}=0^- \Rightarrow \dot{v}^r_{ij}>0$. Here the notation 0^+ (0^-) is used for an infinitesimal positive (negative) number. Clearly, the same conclusion holds in the case $v^r_{ij}=0$ and $\dot{v}^r_{ij} \neq 0$. Thus a nonsliding contact is always obtained as the unique solution, and can be regarded as an attractive fixed point as well. This is valid as long as the signs of the relative velocities at the other contacts do not change. These considerations have important implications in the numerical simulations of the system. Performing a rough numerical integration of the equations of motion (6) and (7) with equidistant time steps $\delta t'$, the situation $v^r_{ij}=0$ will almost never occur. Nevertheless, stable nonsliding contacts $\langle ij \rangle$ can always be detected from an oscillatory behavior of the angular velocities around the fixed point $v^r_{ij}=0$. Furthermore, the simple ansatz

$$T_{ij} = -\mu_{ij}\,\mathrm{sgn}(v^r_{ij})N_{ij}$$

is sufficient for a determination of the friction forces, yielding an enormous simplification for the numerical approach (see Ref. [11]).

First, we have tested this numerical integration procedure for a system consisting of only one cylinder. In its steady state, the cylinder simply rolls on the plane without friction. The numerical results are illustrated in Fig. 5 for a horizontal compression of $N_0+N_1=4$.

Starting the numerical integrations with a negative rotation velocity at $t'=0$, the cylinder's rotation is positively accelerated [$d\omega_1'/dt'=2\mu'$ (cf. Eq. (14))] until $\omega_1'>1$. Just having passed this fixed-point solution, the acceleration changes sign, and the expected oscillations of the angular velocity around the value $\omega_1'=1$ can be observed. Clearly, their amplitude decreases with the time step, since the fluctuations of accelerations and forces are independent of the value of $\delta t'$. In particular, the friction force between the particle and plane changes its direction. Thus, a numerical integration for a fixed value of $N_0<\mu'$ would yield a negative horizontal acceleration of the particle when $\omega_i'>1$. For longer chains with several particles with fixed points at $\omega_i'=1$, the value of N_0 would have to be chosen even larger in

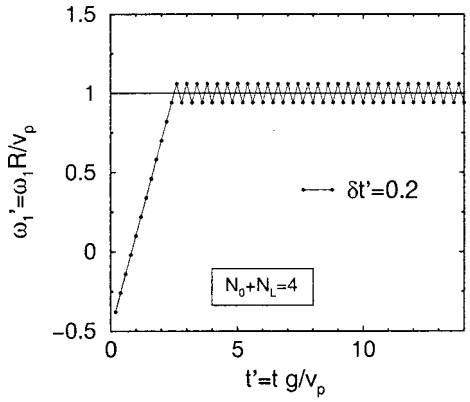

FIG. 5. Temporal evolution of the rotation velocity of one particle ($L=1$) confined by the horizontal compression $N_0+N_1=4$. The friction coefficients are $\mu'=0.3$ and $\mu''=0$.

order to guarantee the close-packing condition of the chain. Thus fixing N_0 as a control parameter will allow one to consider only highly confined chains. The applicability of this numerical procedure is less restricted by choosing the sum of both confining forces, N_0+N_L, as an external parameter instead.

How the algorithm works if the system approaches several nonsliding contacts is presented for a chain with two counter-rotating cylinders. Figure 6 again shows a clear oscillating behavior around the fixed-point solutions $\omega_1'=1$ and $\omega_1'+\omega_2'=0$. The fluctuations of the angular velocities, larger than for the system in Fig. 5, have been reduced by the choice of smaller time steps. Figure 6 shows, that first the counter-rotation of the particles is established. The rotations are then collectively accelerated until the first cylinder simply rolls on the plane. The numerical value of this acceleration, which can be easily estimated from the average slope, is in good quantitative agreement with the analytical prediction derived from Eq. (17): $d\omega_1'/dt'=2\mu'^2=0.18$.

Typical results for a chain of four particles are shown in Fig. 7 for two different horizontal compressions. The oscillating behavior of the curves has been reduced here by the choice of a relatively small integration step of $\delta t'=0.01$. At

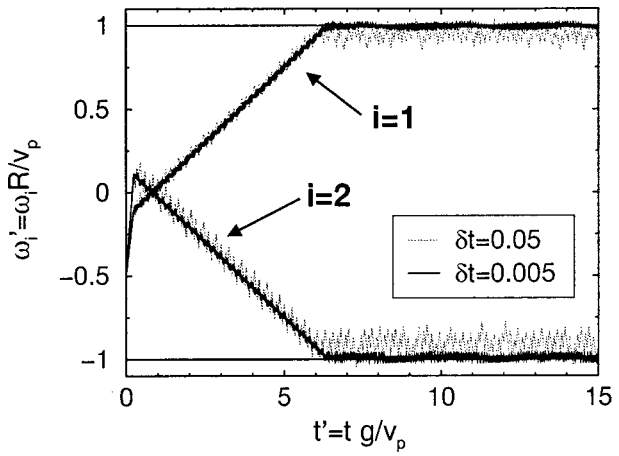

FIG. 6. Temporal evolution of the rotation velocities of two particles ($L=2$) confined by the horizontal compression $N_0+N_L=4$. The friction coefficients are $\mu=0.4$, $\mu'=0.3$, and $\mu''=0$.

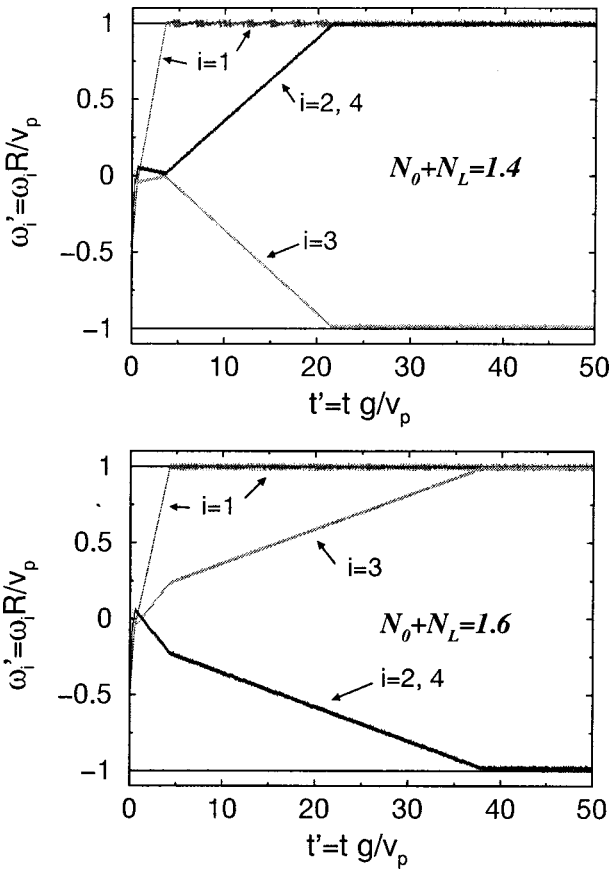

FIG. 7. Temporal evolution of the rotation velocities of four particles ($L=4$) confined by $N_0+N_L=1.4$ (top) and 1.6 (bottom). The friction coefficients are $\mu=0.4$, $\mu'=0.3$, and $\mu''=0$.

both compressions, the first cylinder is positively accelerated until it simply rolls on the plane, whereas a counter-rotating array is built up by the remaining three cylinders. In the counter-rotating region, the rotations of the cylinders are accelerated until the positively accelerated particles roll on the plane without friction. Again, the numerically obtained accelerations are in excellent quantitative agreement with the analytical result [Eq. (17)]. In particular, our prediction of only two angular velocities in the steady state, $\omega_i'=\pm 1$, is confirmed numerically. The values of the horizontal compression determine the spatial arrangement of the rotation velocities. At low confining forces the first two cylinders roll on the plane without friction. At high compression all particles act in a counter-rotating mode.

We conclude that the simple molecular-dynamics code [11] presented here yields reliable results for the temporal evolution of the angular velocities as well as for the steady-state properties. The same rotation patterns are obtained for a regularized version of Coulomb's law, as used in Ref. [4], with reduced fluctuations of the angular velocities due to the regularization of the friction forces in the vicinity of vanishing relative contact velocities.

The different steady-state patterns with only two phases (I, and III) are determined by the length of the first phase, L_1. Each value of L_1 corresponds to a certain range of the horizontal compression of the chain.

The real transition time T_{trans} to the steady state can be simply obtained from its value T'_{trans} in the simulations:

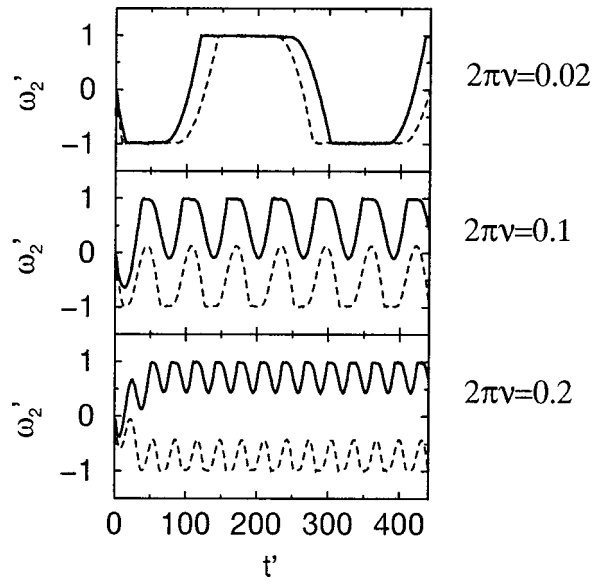

FIG. 8. Temporal evolution of the rotation velocities of the second of four particles ($L=4$) confined by $N_0+N_L=\langle N_0+N_L\rangle+0.2\cos(2\pi\nu t')$, with straight lines for $\langle N_0+N_L\rangle=1.5$ and dotted lines for $\langle N_0+N_L\rangle=1.58$. The friction coefficients are $\mu=0.4$, $\mu'=0.3$, and $\mu''=0$. The integration steps are chosen as $\delta t'=0.015$.

$T_{trans}=T'_{trans}v_p/g$. In the experiment, the velocity of the basal plane is small, $v_p<10^{-4}$ m/s, yielding $T^{exp}_{trans}<T'_{trans}\times 10^{-5}$ s. Numerically, we have observed that typically $T'_{trans}\ll 10^3$; thus the transition time in the experiment can be expected to be very short: $T^{exp}_{trans}\ll 10^{-2}$ s.

We now turn to a numerical investigation of the chain's reaction on temporally fluctuating horizontal compressions. To this end, we assume periodic oscillations of the confining forces:

$$N_0+N_L=\langle N_0+N_L\rangle+A\cos(2\pi\nu t').$$

As a consequence, the horizontal compression switches between the ranges of the different steady-state patterns for constant compression. Thus simple oscillations between these steady states can be expected for frequencies with a periodicity time larger than T'_{trans}. For higher frequencies, the situation is less obvious. We have studied the situation for the chain in Fig. 7, choosing $A=0.2$ and two different average compressions. For all frequencies, we observed that, after a very short transition time, the first particle rolls on the plane with $\omega_1=1$, and the three remaining cylinders act in a counter-rotating mode. Thus it is sufficient to consider the temporal evolution of one of the counter-rotating cylinders.

In Fig. 8, the temporal evolution of the angular velocities of the second cylinder is represented for three different frequencies ν. For a low frequency, $T'_{trans}\ll 1/(2\pi\nu)$ (top), its angular velocity is observed to switch between $\omega'_2=1$, when N_0+N_L is small, and $\omega'_2=-1$ for large N_0+N_L. Accordingly, the whole chain switches between the two different steady states in Fig. 7. This is exactly what was predicted above. The difference of the value of the average compression, $\langle N_0+N_L\rangle$, only slightly affects the time the chain remains in its different steady-state patterns.

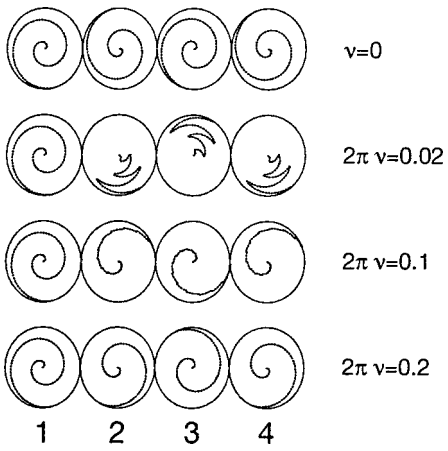

FIG. 9. Polar representation of the temporal evolution of the rotation angles for the same chain as in Fig. 8, confined by $N_0+N_L=1.58+0.2\cos(2\pi\nu t')$.

The situation changes drastically, when the periodicity of the external compression approaches T'_{trans} (center of Fig. 8). The particle remains mainly in its dominant steady state [$\omega'_2=1(-1)$ for $\langle N_0+N_L\rangle=1.5(1.58)$]. The transition time is now too long for a switch between these two states. This effect becomes more pronounced for a higher frequency (see the bottom of Fig. 8). Here, the oscillations of the compression only provoke slight perturbations of the angular velocities.

To summarize, the effects of temporal oscillations of the horizontal compression are largest for small frequencies. They diminish with increasing frequency.

In Fig. 9, the polar representation of the rotation angles for the situation of Fig. 8 is shown with $\langle N_0+N_L\rangle=1.58$. A qualitative comparison with the feature of the experimental curves in Fig. 2 shows that the experimentally observed oscillations of the rotation angle at the right end of the chain can in fact be recovered theoretically for the smallest frequency $2\pi\nu=0.02$.

We have performed numerical simulations for a longer chain with several different steady states. The results are shown in the polar representation in Figs. 10 and 11. The effects are only small for the higher frequency in Fig. 10, whereas convincing agreement with the typical features of the experimental results is found for small values of ν (Fig. 11). In Fig. 11, not only the oscillations of the rotation angles are clearly detected. An intermediate behavior can also be observed for $i=3$. To summarize, in the long-time behavior, oscillations of the confining forces may have an important influence on the rotational patterns as long as the confining forces pass the threshold values between different steady-

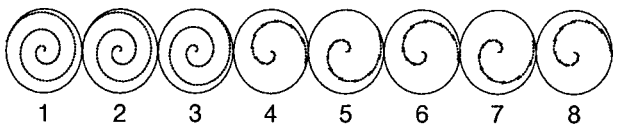

FIG. 10. Rotation angles as a function of t' for a chain of eight cylinders with friction coefficients $\mu=\mu'=0.2$ and $\mu''=0$. The external compression is $N_0+N_L=1.8+0.1\cos(2\pi\nu t')$, with $2\pi\nu=5\times 10^{-3}$. The width of the $N_{t'}=5\times 10^5$ integration steps is $\delta t'=0.033$.

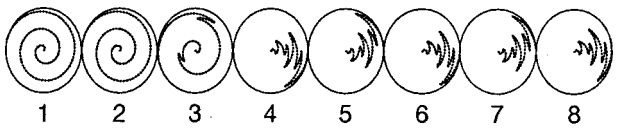

FIG. 11. The same as Fig. 10 for $2\pi\nu = 10^{-3}$.

state patterns. This influence is largest when the time the compression remains in the range of one steady-state pattern is larger than its typical transition time. Our numerical integrations show that, at high frequencies, when these times are smaller than the typical transition time, the chain chooses one dominant pattern. In this case, the fluctuations of the compression only yield slight perturbations of the rotation velocities $\pm\omega_p$ at this state. The amplitude of these oscillations reduces with increasing frequency ν of the compression's oscillations. At low frequencies, when $2\pi\nu \ll 1/T'_{trans}$, the chain ''switches'' between different steady-state patterns. These switches evoke changes of the parity of the length of the counter-rotating array (phase III). Consequently, the rotation velocities of the cylinders at the end of the chain change sign, yielding the experimentally observed oscillations of the rotation velocities (cf. Fig. 2). The intermediate behavior in the middle of the chain can then be understood as a superposition in time of phases I and III.

We conclude that for irregular fluctuations of the compression, the low-frequency variations mainly determine the variations of the rotational patterns. Their high-frequency contribution only evokes slight perturbations of the dominant behavior.

IV. EXPERIMENTAL RESULTS II: TEMPORAL CORRELATIONS

In Sec. III, we showed that the striking unusual properties of the experimental data can be attributed to slowly varying temporal fluctuations of the horizontal compression. This can happen whenever the time scale of these slow fluctuations is much larger than the transition time T_{trans} of the experimental system. Based on our numerical results, the typical transition time of the system could be estimated to be very short: $T_{trans} \ll 10^{-2}$ s; thus all fluctuations with a larger time scale yield superpositions of different steady-state patterns.

In this section, we will analyze temporal correlations of the experimentally observed fluctuations of the rotation angles. Such an analysis requires a higher precision of our angle measurements. The precision is restricted by the image analysis. Zooming in on the front of only one cylinder of the chain, we obtain a reduced maximum error of 0.4° for the measured angles. A typical experimental result for the cylinder $i=7$ of a chain of $L=9$ cylinders is shown in Fig. 12. The chain has been confined by a cardboard block of 23.8 g. All the other experimental parameters are the same as in Figs. 2 and 3.

The irregular shape of the curves reminds one of a signal obtained from a stochastic process. Whereas the total rotation angles $\Theta(t)$ show a nonstationary behavior, a stationary process seems to fit the short-time rotation angles $\Delta\Theta(t) = \Theta(t+\Delta t) - \Theta(t)$ between two snapshots ($\Delta t = 9$ s). These ''instantaneous'' rotational measurements correspond

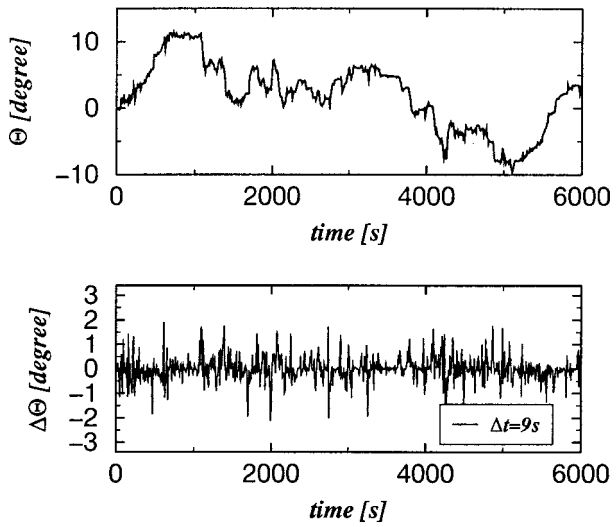

FIG. 12. Time dependence of the experimentally measured rotation angles of cylinder $i=7$ for a chain with $L=9$. Top: total rotation angles; bottom: rotation angles between two snapshots.

to running averages of the velocities in this time interval. In order to compare directly with the theory, the instantaneous angular velocities of the cylinder would be needed. These velocities, however, are not accessible in the experimental measurements. Therefore, the moving averages will be the basis of our analysis. The maximum rotation velocity ($|\omega_p| \simeq 0.34°/\mathrm{s}$) corresponds to a rotation angle of $\Delta\Theta \simeq \pm 3.1°$ between two snapshots. This angle is only rarely observed in the experiment. However, as discussed at the end of Sec. III, instantaneous rotation velocities much smaller than $\pm\omega_p$ can be expected to give a negligible contribution. Thus the experimental data presented in Fig. 12 give rise to several switches of sign of the rotation velocity in the time interval $\Delta t = 9$ s.

In order to gain a deeper insight into the temporal correlations of the experimental data, we have computed their autocorrelation function as well as their power spectrum. These functions offer excellent statistical tools for the detection of characteristic properties of an irregular signal.

The autocorrelation function A_f of a time series $f(t_i)$ measured in equidistant time steps δt at times t_i, $i = 1, \ldots, N$, can be estimated from

$$A_f(\tau = k\delta t) \simeq c_k / c_0,$$

with

$$c_k = \frac{1}{N-k} \sum_{i=1}^{N-k} [f(t_{i+k}) - \overline{f}][f(t_i) - \overline{f}]. \tag{21}$$

Here $\overline{f} = (1/N)\Sigma_{i=1}^{N} f(t_i)$ is the sample mean of f (cf. Ref. [12]), and c_k is the estimated autocovariance.

A hidden periodicity of an irregular signal f can be detected from peaks of $A_f(\tau)$ at integer multiples of its periodicity time. On the other hand, for random values of $f(t)$, generated by a stationary uncorrelated process, $A_f(\tau)$ vanishes for all values $\tau > 0$. At $\tau = 0$, one always obtains $A_f(0) = 1$.

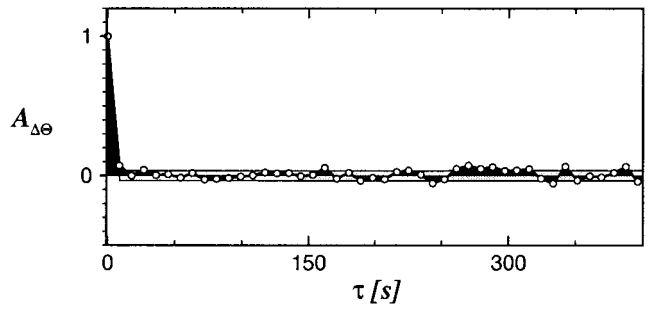

FIG. 13. Estimated autocorrelation function of the instantaneous rotation angles presented in Fig. 12 (bottom).

The autocorrelation function estimated from the instantaneous rotation angles in Fig. 12 (bottom) is represented as a function of τ in Fig. 13. We have restricted our representation to relatively small values of τ compared with the total measuring time for which our estimate is expected to give reliable results. For the mean rotation velocities between two snapshots, no significant correlations can be detected for $\tau \geqslant \Delta t$.

Clearly, a more or less regular oscillating behavior can be excluded on the basis of these results. The small values of $A_{\Delta\Theta}$ for $\tau \geqslant \delta t$ in Fig. 13 more likely suggest that one think in terms of random velocities generated from a stationary stochastic process (*random walk*). The mean error of an estimated autocorrelation which theoretically vanishes for all lags $k>q$ can be calculated from Bartlett's approximation [13]. It enables us to detect systematic deviations from a random-walk behavior. This error, represented as a gray bar around zero, covers most of the calculated nonvanishing values in Fig. 13, and no apparent contradiction to our hypothesis can be detected. Moreover, we can see the f^{-2} variation of the power spectrum $S_f=|\tilde{\Theta}(f)|^2$,

$$\tilde{\Theta}(f)=\frac{1}{T}\int_0^T dt\, e^{i2\pi ft}\Theta(t),$$

shown in Fig. 14, typical behavior for a random walk [14].

We conclude from our results that the temporal fluctuations of the horizontal confinement of the chain can best be

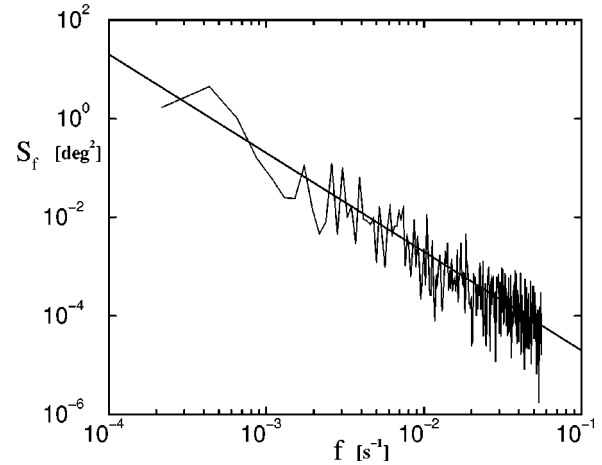

FIG. 14. Power spectrum of experimental data presented in Fig. 12.

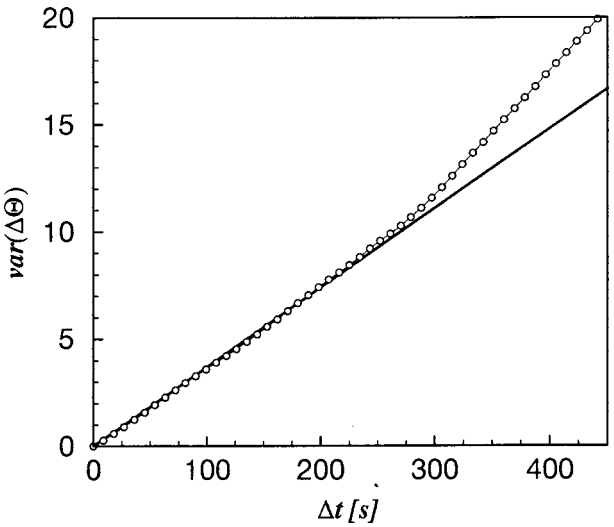

FIG. 15. Estimated variance of the short-time rotation angles $\Delta\Theta$ (degree) as a function of Δt.

described in terms of a stationary stochastic process. Whenever the time between two events is not of the order of T^{trans}, this corresponds to a random superposition of the steady-state rotation velocities $\pm\omega_p$.

In a random-walk system, the mean squared displacement increases linearly in time (cf., e.g., Refs. [15,16]), i.e.,

$$\langle[\Theta(t)-\langle\Theta(t)\rangle]^2\rangle=2Dt.$$

The slope of this function is completely determined by the diffusion constant D, from which further insight into the ''microscopic'' properties of the process can be gained. The stationarity of the process implies that this relation also holds for $\Delta\Theta(\Delta t)$. We have estimated the variance of $\Delta\Theta(\Delta t)$ from the autocovariance c_0 in expression (21). The result, presented in Fig. 15, shows a remarkably linear increase up to $\Delta t \approx 300$ s. For larger times, the slope is increased only by statistical deficiency, not by real physical correlations. The slope of the straight line is $2D \approx 0.04$ degrees^2/s. In order to exploit the information obtainable from this value, assumptions on the temporal distribution of the random events have to be made. Since no further information is available, we assume the random events at random times. With this assumption we follow the standard lines for diffusion by collisions in an ideal gas. For further details see, e.g., Ref. [16]. Now the diffusion constant can be derived from the ''microscopic'' processes. The result,

$$D=(\overline{\omega^2}-\overline{\omega}^2)\,\overline{\tau}, \tag{22}$$

relates D to the mean time interval between two events, $\overline{\tau}$, and the variance of the instantaneous rotation velocities, $\overline{\omega^2}-\overline{\omega}^2$. Furthermore, our assumption of random times for the events enables us to derive an exact expression for the distribution of time intervals τ between two events [16]:

$$P(\tau)=\frac{1}{\tau}\exp(-\tau/\overline{\tau}). \tag{23}$$

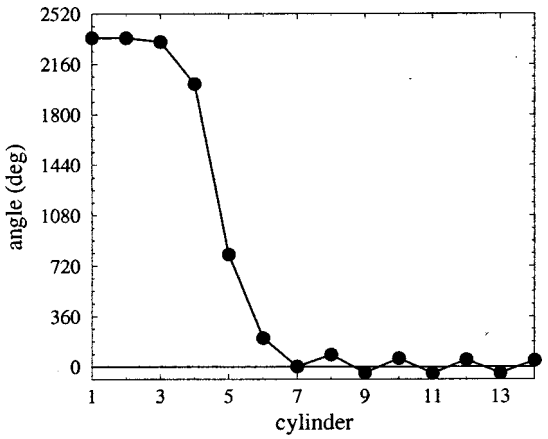

FIG. 16. Measured total rotation angles for a chain of 14 cylinders.

From the slope in Fig. 15 and $\overline{\omega^2}-\overline{\omega}^2 \leqslant \overline{\omega_p^2}$ ($\overline{\omega} \simeq 0$), we obtain $\overline{\tau} \geqslant 0.16$ s. Making use of expression (23), we can check now the consistency of our assumptions. The percentage of time intervals shorter than a very large transition time of 10^{-2} s is small ($\approx 6\%$), thus strongly supporting the existence of mainly two instantaneous rotation velocities $\pm\omega_p$ in the experiment. On the other hand, the percentage of events on a time scale larger than the distance between two snapshots ($\tau \geqslant 9$ s) is negligible ($\sim 10^{-24}\%$). This explains, why the maximum rotation angle of $\pm 3.1°$ cannot be detected in Fig. 12.

It appears clearly that the length of phase I oscillates during time. The total measured rotation angle of each cylinder is the result of the superposition of different steady states (Fig. 1), with perfectly known spatial correlations. The first particles are in phase I and are rolling with the same velocity $+\omega_p$, the first particle in phase III has a velocity $-\omega_p$, and the velocities of the others are alternating between $+\omega_p$ and $-\omega_p$.

So, with this description, the distribution of lengths of phase I is completely determined by the knowledge of the total angles $\Theta(n)$ of each cylinder $n=1,\ldots,L$ during the experiment (Fig. 16). We can easily compute the fraction in time of each steady state giving the length distribution of phase I.

Our hypothesis of instantaneous steady-state velocities gives us a few recurrence relations between the different time fractions: $t_I(n)$, $t_{III}^{+}(n)$, and $t_{III}^{-}(n)$, respectively, are the fractions of time during which the cylinder n is in phase I, in phase III with the velocity $+\omega_p$, and in phase III with the velocity $-\omega_p$. Θ_{max} is the total rotation angle of a cylinder which always is in phase I. Then we obtain

$$\frac{\Theta(n)}{\Theta_{max}} = t_I(n) + t_{III}^{+}(n) - t_{III}^{-}(n), \tag{24}$$

with

$$t_I(n) + t_{III}^{+}(n) + t_{III}^{-}(n) = 1 \tag{25}$$

and

$$t_{III}^{+}(n) = t_{III}^{-}(n-1). \tag{26}$$

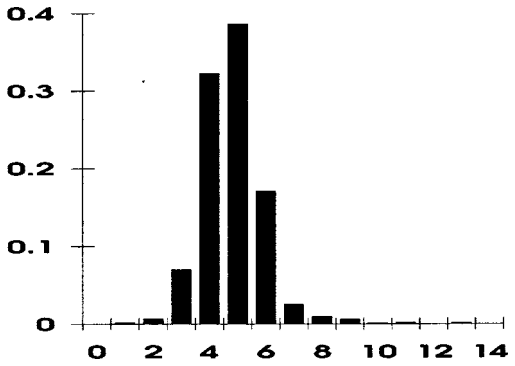

FIG. 17. Length distribution $p(L_1)$ of the phase I for the experiment presented in Fig. 16.

With the $t_I(n)$ values we can deduce the time fraction $p(L_1)$ when phase I has a length of L_1 cylinders. $p(L_1)$ is simply given by

$$p(L_1) = t_I(L_1) - t_I(L_1+1). \tag{27}$$

The length distribution $p(L_1)$ of phase I for the experimental data presented in Fig. 16 (14 plexiglas cylinders, $v_p = 125$ μm/s, 7.5 g confining mass) is shown in Fig. 17.

We conclude that the results of our numerical integrations for oscillating confining forces, together with the analysis of the temporal correlations of the experimentally measured rotation angles, strongly support our hypothesis—that the unexpected properties of the experimental data can be traced back to random superpositions of different steady-state rotation patterns. There is strong evidence that the chain performs a *collective random walk.*

V. CONCLUSIONS

To summarize, the striking unexpected properties of our experimental measurements can be—qualitatively and quantitatively—attributed to slow varying temporal fluctuations of the chain's horizontal confinement. In detail, we showed, by means of rigorous analytical derivations, that the steady state of the perfect nonaccelerated system has only two rotation velocities, $\pm\omega_p$. Only two rotational modes, phases I and III, exist in this case. The molecular-dynamics code developed here shows an excellent quantitative agreement with the derived rigorous analytical results. From our numerical simulations, the typical transition time to the steady state could be estimated to be very short for the experimental situation. Slowly varying oscillations of the chain's horizontal compression yield temporal superpositions of different steady-state patterns. For periods smaller than the transition time of the system, the rotation patterns are only weakly affected by these external fluctuations: the dominant steady-state pattern is obtained with slight fluctuations of the rotation velocities. The amplitude of these fluctuations diminishes with increasing frequency. The typical features of our experimental measurements are reproduced by numerical simulations with slow-frequency oscillations of the confining forces.

Further insight into the experimentally measured fluctua-

tions of the rotation velocities could be gained from a computation of the temporal autocorrelation function and the power spectrum. The temporal correlations are best described by a one-dimensional random walk of the cylinders. Based on our estimated diffusion constant, short-time fluctuations are found to give a small contribution only, strongly supporting the supposition that the measured data are a consequence of temporal superpositions of different steady-state patterns.

ACKNOWLEDGMENTS

We are very grateful to R. Delannay for his support in theoretical questions, and for his very good idea to describe the motion of a particle in phase III as a random walk. It is a pleasure to acknowledge many stimulating discussions with D. Bideau, L. Oger, and A. Valance. G.S. acknowledges financial support from the CNRS, and hospitality from University of Rennes 1.

[1] *Friction, Arching, Contact Dynamics*, edited by D. E. Wolf and P. Grassberger (World Scientific, Singapore, 1997).
[2] D. Wolf, in *Physics of Dry Granular Media*, edited by H. J. Herrmann, J.-P. Hovi, and S. Luding (Kluwer, Dordrecht, 1998).
[3] F. Radjai and S. Roux, Phys. Rev. E **51**, 6177 (1995).
[4] F. Radjai, J. Schaefer, S. Dippel, and D. Wolf, J. Phys. I **7**, 1053 (1997).
[5] F. Radjai, P. Evesque, D. Bideau, and S. Roux, Phys. Rev. E **52**, 5555 (1995).
[6] Y. Khidas, G. Schliecker, M. Ammi, J. C. Messager, and R. Delannay, Europhys. Lett. (to be published).
[7] C. Coulomb, Mémoire de Mathématiques Physique l'Académie Royale **10**, 161 (1785).
[8] M. Jean, *Mechanics of Geometrical Interfaces* (Elsevier, New York, 1994).
[9] T. Baumberger and C. Caroli, MRS Bull. **23**, 41 (1998).
[10] F. Radjai, L. Brendel, and S. Roux, Phys. Rev. E **54**, 861 (1996).
[11] J. Schaefer, S. Dippel, and D. E. Wolf, J. Phys. I **6**, 5 (1996).
[12] G. E. P. Box, G. M. Jenkins, and G. C. Reinsel, *Time Series Analysis* (Prentice Hall, Englewood Cliffs, NJ, 1994).
[13] M. S. Bartlett, J. R. Stat. Soc. B **8**, 27 (1946).
[14] F. J. Molz, H. H. Liu, and J. Szulga, Water Resour. Res. **33**, 2273 (1997).
[15] P. M. Chaikin and T. C. Lubensky, *Principles of Condensed Matter Physics* (Cambridge University Press, Cambridge, 1995).
[16] F. Reif, *Fundamentals of Statistical and Thermal Physics* (McGraw-Hill, Singapore, 1985).